

Open-Framework Borophosphates: (NH₄)_{0.4}Fe^{II}_{0.55}Fe^{III}_{0.5}(H₂O)₂[BP₂O₈]·0.6H₂O and NH₄Fe^{III}[BP₂O₈(OH)]

Ya-Xi Huang,^{†,‡} Gerd Schäfer,[†] Wilder Carrillo-Cabrera,[†] Raul Cardoso,[†]
Walter Schnelle,[†] Jing-Tai Zhao,^{†,‡} and Rüdiger Kniep^{*,†}

Max-Planck-Institut für Chemische Physik fester Stoffe, Nöthnitzer Strasse 40,
01187 Dresden, Germany, and College of Chemistry and Chemical Engineering,
Xiamen University, 361005 Xiamen, P. R. China

Received April 12, 2001. Revised Manuscript Received August 14, 2001

Two open-framework ammonium–iron borophosphates, black colored (NH₄)_{0.4}Fe^{II}_{0.55}Fe^{III}_{0.5}(H₂O)₂[BP₂O₈]·0.6H₂O (**1a**) (pale gray colored **1b** with a powder X-ray diffraction pattern indicating an isotype relationship was also observed) and pale pink colored NH₄Fe^{III}[BP₂O₈(OH)] (**2**), were synthesized under mild hydrothermal conditions at 180 °C. Their crystal structures were determined by single-crystal X-ray investigations (hexagonal, *P6₅* (no. 170), *a* = 9.483(4) Å, *c* = 15.697(5) Å, *V* = 1222.5(8) Å³, and *Z* = 6 for **1a** and monoclinic *P2₁/c* (no. 14), *a* = 9.370(1) Å, *b* = 8.309(2) Å, *c* = 9.680(1) Å, *β* = 102.05(1)°, *V* = 737.0(2) Å³, and *Z* = 4 for **2**, respectively). The crystal structure of **1a** is characterized by corner-sharing PO₄ and BO₄ tetrahedra, leading to infinite helical ¹_∞{[BP₂O₈]³⁻} ribbons, which are connected by Fe^{II/III}O₄(H₂O)₂ coordination octahedra. An additional trigonal bipyramidal Fe^{II/III}O₂(H₂O)₃ coordination polyhedron shares common corners and edges with three Fe^{II/III}O₄(H₂O)₂ coordination octahedra, leading to tetrameric units. Helical channels, running along [001], are statistically occupied by H₂O molecules and NH₄⁺ ions. The structure of **2** is characterized by an infinite ¹_∞{[BP₂O₈(OH)]⁴⁻} chain, which is further connected by Fe^{III}O₄(H₂O)₂ coordination octahedra leading to one-dimensional channels which are occupied by NH₄⁺ ions. The magnetic properties of both compounds are presented. For compound **1a** (and **1b**), the mixed-valence state of iron was confirmed. The susceptibility of compound **2** reveals a stronger magnetic interaction and an antiferromagnetic ordering at 17 K.

Introduction

Compounds with open-framework structures are of great interest in material science, as well as in chemistry, due to their applications as catalysts, ion-exchangers, or molecular sieves.¹ Open-framework borophosphates are potential materials for heterogeneous catalysis, as shown for BPO₄.² Although systematic investigations on borophosphates began only a few years ago, a broad spectrum of compounds has already been characterized with various anionic partial structures such as oligomeric units, chains, ribbons, layers, and three-dimensional frameworks.^{3–6} The possibility of creating more open structures by using organic templates was also demonstrated.^{7–9}

Asymmetric catalysis using chiral porous materials or chirally modified metals has become an important research field.¹⁰ A chiral octahedral–tetrahedral framework, related to the *CZP* topology,¹¹ is present in the crystal structures of a family of borophosphates with the general formula A^I_{*x*}M^{II}_{*y*}(H₂O)₂[BP₂O₈]_{*z*}·*z*H₂O (A^I = Li, Na, K, Rb, Cs; M^{II} = Mg, Mn, Fe, Co, Ni, Cu, Zn; *x* = 0.35–1, *y* = 1–1.3, *z* = 0.2–1)^{12,13} with a remarkable reversible dehydration process, leading to microporous chiral compounds, among which NaZn(H₂O)₂[BP₂O₈]·H₂O was investigated in detail.¹⁴ Recently, the existence of a pure iron(III) compound Fe(H₂O)₂[BP₂O₈]·H₂O, which exhibited the same structure type, was described.¹⁵ Comments on this observation will be given below. Here we report on a new member of this family,

* To whom correspondence should be addressed. E-mail: kniep@cpfs.mpg.de.

[†] Max-Planck-Institut für Chemische Physik fester Stoffe.

[‡] Xiamen University.

(1) Cheetham, A. K.; Férey, G.; Loiseau, T. *Angew. Chem., Int. Ed.* **1999**, *38*, 3268.

(2) *Gmelin Handbuch der Anorganischen Chemie*; Springer: Berlin, Heidelberg, New York, 1975; Vol. 19, Part 3, pp 99–106.

(3) Kniep, R.; Engelhardt, H.; Hauf, C. *Chem. Mater.* **1998**, *10*, 2930.

(4) Kniep, R.; Schäfer, G.; Engelhardt, H.; Boy, I. *Angew. Chem., Int. Ed.* **1999**, *38*, 3641.

(5) Bontchev, R. P.; Do, J.; Jacobson, A. J. *Angew. Chem., Int. Ed.* **1999**, *38*, 1937.

(6) Bontchev, R. P.; Do, J.; Jacobson, A. J. *Inorg. Chem.* **2000**, *39*, 3320.

(7) Sevov, S. C. *Angew. Chem., Int. Ed. Engl.* **1996**, *35*, 2630.

(8) Kniep, R.; Schäfer, G. *Z. Anorg. Allg. Chem.* **2000**, *626*, 141.

(9) Schäfer, G.; Borrmann, H.; Kniep, R. *Z. Anorg. Allg. Chem.* **2001**, *627*, 61.

(10) Bein, T. *Curr. Opin. Solid State Mater. Sci.* **1999**, *4*, 85.

(11) Baerlocher, C.; McCusker, L. B. *Atlas of Zeolite Structure Types*. <http://www.iza-structure.org/databases>.

(12) Boy, I.; Kniep, R. *Z. Kristallogr. NCS* **2001**, *216*, 9.

(13) Kniep, R.; Will, H. G.; Boy, I.; Röhr, C. *Angew. Chem., Int. Ed. Engl.* **1997**, *36*, 1013.

(14) Boy, I.; Stowasser, F.; Schäfer, G.; Kniep, R. *Chem.–Eur. J.* **2001**, *7*, 834.

(15) Yilmaz, A.; Bu, X.; Kizilyalli, M.; Stucky, G. D. *Chem. Mater.* **2000**, *12*, 3243.

Table 1. Ammonium–Iron Borophosphates 1a, 1b, and 2: Results of Chemical Analyses in Mass % (see text); (esd)

reaction product (color)	Fe obsd/calcd ^a	B obsd/calcd	P obsd/calcd	N obsd/calcd
1a (black)	19.86(20)/18.71	3.430(4)/3.45	19.99(6)/19.76	2.82(16)/1.79
1b (pale gray)	20.23(13)/18.71	3.402(1)/3.45	19.64(15)/19.76	2.73(18)/1.79
2 (pale pink)	19.72(8)/19.15	3.53(5)/3.71	21.33(38)/21.24	4.55(21)/4.80

^a The values were calculated for **1a** and **1b**, assuming a composition of $(\text{NH}_4)_{0.4}\text{Fe}^{\text{II}}_{0.55}\text{Fe}^{\text{III}}_{0.5}(\text{H}_2\text{O})_2[\text{BP}_2\text{O}_8]\cdot 0.6\text{H}_2\text{O}$ (result of the single-crystal structure determination).

$(\text{NH}_4)_{0.4}\text{Fe}^{\text{II}}_{0.55}\text{Fe}^{\text{III}}_{0.5}(\text{H}_2\text{O})_2[\text{BP}_2\text{O}_8]\cdot 0.6\text{H}_2\text{O}$ (**1a**), and on a second compound, $\text{NH}_4\text{Fe}^{\text{III}}[\text{BP}_2\text{O}_8(\text{OH})]$ (**2**), with $\text{M}^{\text{I}}\text{M}^{\text{III}}[\text{BP}_2\text{O}_8(\text{OH})]$ ($\text{M}^{\text{I}} = \text{Rb}, \text{Cs}; \text{M}^{\text{III}} = \text{V}, \text{Fe}$) structure type.¹⁶

Experimental Section

Syntheses and Chemical and Thermal Analyses. The title compounds were synthesized under mild hydrothermal conditions. A 5.675 g (28.5 mmol) portion of $\text{FeCl}_2\cdot 4\text{H}_2\text{O}$ (Merck, $\geq 99\%$), 7.550 g (57 mmol) of $(\text{NH}_4)_2\text{HPO}_4$ (Merck, $\geq 99\%$), and 1.758 g (28.5 mmol) of H_3BO_3 (Roth, $\geq 99.9\%$) were mixed together in 10 mL of deionized water with stirring. A 7.753 g portion of 85% H_3PO_4 (Merck, p.a.) was added after the mixture was homogenized. The resulting gray gel was transferred to a Teflon autoclave ($V = 20$ mL; degree of filling $\approx 70\%$; $\text{pH} = 1.0\text{--}1.5$) and held at 180°C for 3 days. The reaction products were separated by vacuum filtration, washed with deionized water, and dried for 1 day at 60°C . Three kinds of crystals were separated from this reaction: black crystals (purple colored in transmitted light) with hexagonal bipyramidal and trapezoidal shape (**1a**), pale gray translucent crystals with the same shape (**1b**), and pale pink translucent rod-shaped crystals (**2**). The relative amount of the reaction products can be controlled by the experimental conditions. These are stirring time (preparation of the reaction gels), reaction temperature, reaction time, pH value, and degree of filling of the autoclave. Among these, reaction temperature is the most important factor. At $100\text{--}140^\circ\text{C}$, the small pale gray crystals of **1b** constitute the main part of the product, while at 180°C , larger black crystals of **1a** were found as the majority phase, and at 220°C , pale pink crystals of **2** were found together with black opaque aggregates of $\text{NH}_4\text{Fe}_2(\text{PO}_4)_2$.¹⁷

Both the differently colored crystals with hexagonal morphology (**1a** and **1b**) showed the same X-ray powder diffraction pattern (Huber Image-Foil Guinier-Camera G670, $\text{Co K}\alpha_1$ radiation, curved quartz (101) monochromator), matching the calculated diffraction pattern of **1a**. The pale pink rod-shaped crystals were assigned to **2** with the same method.

Iron, boron, and phosphorus contents of the three reaction products **1a**, **1b**, and **2** were analyzed by ICP-AES (Varian Vista RL), while nitrogen contents were analyzed with a carrier gas hot extraction method (Leco TC-436 DR, furnace EF 500). For experimental and calculated analytical data, see Table 1. The observed contents of nitrogen in **1a** and **1b**, which are significantly higher than the calculated ones, should be treated as semiquantitative values because of the analytical method used here but generally prove the presence of nitrogen.

Thermal properties were investigated using DTA/TG methods in a static air atmosphere with heating and cooling rates of 5°C min^{-1} (Netzsch STA 409 EP). For the black colored reaction product **1a**, a three-step mass loss of 15.53% (calcd 17.18%, by assuming a total loss of H_2O and NH_3) was observed. The pale gray reaction product **1b** showed a similar thermal behavior with a total mass loss of 15.45% in three steps. The last step in both TG curves in the temperature range of $500\text{--}700^\circ\text{C}$ —a typical temperature range for the release of NH_3 —is slightly different for the reaction products **1a** (2.87%) and **1b** (2.39%), respectively. Compound **2** shows a one-step mass loss of 11.92% (calcd 12.02%). According to

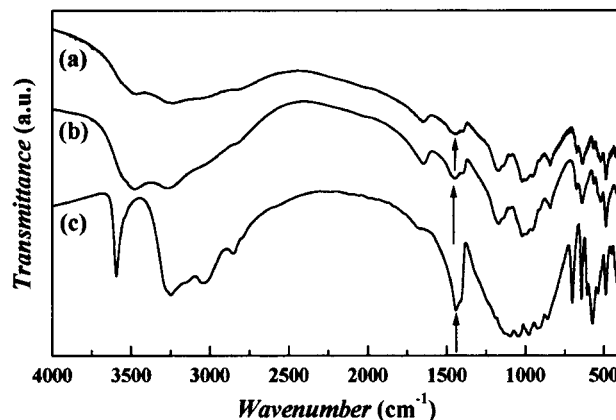


Figure 1. FT-IR spectra of **1a** (a), **1b** (b), and **2** (c). The positions of the ν_4 N–H deformation vibrations are marked with arrows.

the X-ray powder diffraction measurements, the products of all three thermal decomposition reactions are α - BPO_4 and unidentified phases.

IR Spectroscopy. FT-IR spectra of reaction products **1a**, **1b**, and **2** were collected to confirm the presence of O–H and N–H moieties (Bruker IFS 66v/S). The spectra of **1a** and **1b** show similar absorption bands [**1a**: O–H stretching (3482 cm^{-1}), ν_3 (N–H) (3267 cm^{-1}), O–H deformation (1643 cm^{-1}), ν_4 (N–H) (1448 cm^{-1}); **1b**: O–H stretching (3478 cm^{-1}), ν_3 (N–H) (3260 cm^{-1}), O–H deformation (1643 cm^{-1}), ν_4 (N–H) (1445 cm^{-1})]. Both spectra verify the presence of NH_4^+ ions which are necessary for the charge balance together with the iron present in mixed valence states, as can already be assumed by the product colors alone. The spectrum of **2** [O–H stretching (3594 cm^{-1}), ν_3 (N–H) (3248 cm^{-1}), ν_1 (N–H) (3042 cm^{-1}), $2\nu_4$ (N–H) (2852 cm^{-1}), O–H deformation (1676 cm^{-1}), ν_4 (N–H) (1442 cm^{-1})] shows a very sharp peak for the O–H vibration, precluding a O–H \cdots O or O–H \cdots N hydrogen bond for the B–O–H hydroxyl group (Figure 1).

Magnetic Susceptibility. The magnetizations of all three reaction products were measured with a SQUID magnetometer (Quantum Design MPMS-XL 7) in the temperature range of $1.8\text{--}350\text{ K}$ (Figure 2). For **1a** and **1b**, the data of the magnetic susceptibility follow the Curie–Weiss law over almost the whole measured temperature range with small deviations below 50 K (external magnetic field $H_{\text{ext}} = 10\text{ kOe}$). The effective magnetic moments μ_{eff} were calculated by a nonlinear fit in the range of $50\text{--}350\text{ K}$ to $5.58\mu_{\text{B}}/\text{Fe-atom}$ (**1a**, $\Theta = -3.8\text{ K}$) and $5.69\mu_{\text{B}}/\text{Fe-atom}$ (**1b**, $\Theta = -4.0\text{ K}$), respectively. Both values are between typical values for high-spin Fe^{II} and Fe^{III} , confirming the mixed-valent state of iron in both compounds. The slightly different values for the magnetic moments can explain the different colors of the product and may indicate a different ratio of Fe^{II} and Fe^{III} . The magnetic susceptibility of **2** is strongly different from that of **1a** and **1b**. The effective magnetic moment value $\mu_{\text{eff}} = 5.88\mu_{\text{B}}/\text{Fe-atom}$ fits typical values for pure high-spin Fe^{III} compounds ($5.8\text{--}6.0\mu_{\text{B}}/\text{Fe-atom}$). Even more significant is the much larger absolute value of the Weiss constant ($\Theta = -60\text{ K}$), indicating strong antiferromagnetic interaction between the Fe^{III} ions. At low temperatures, deviation from Curie–Weiss behavior is observed. At $\approx 22\text{ K}$, the susceptibility in a field of 10 kOe displays a round maximum and decreases with decreasing temperature. A clear cusp at 17 K indicates an antiferromagnetic ordering of the

(16) Knip, R.; Boy, I.; Engelhardt, H. *Z. Anorg. Allg. Chem.* **1999**, *625*, 1512.

(17) Boudin, S.; Lii, K.-H. *Inorg. Chem.* **1998**, *37*, 799.

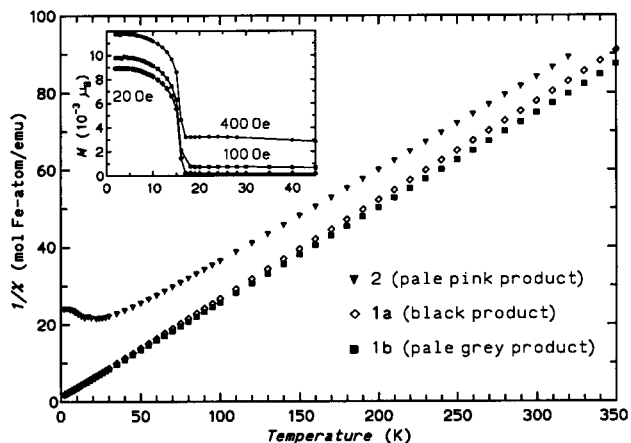


Figure 2. Inverse molar magnetic susceptibilities for the three reaction products **1a**, **1b**, and **2** (external field 10 kOe) and, in the inset, the magnetization of **2** in different external fields.

Fe^{III} ions. Magnetization data in lower external fields (inset of Figure 2) display antiferromagnetic ordering at $T_N \approx 17$ K. The presence of a weak ferromagnetic component of $\approx 10^{-2} \mu_B/\text{Fe-atom}$ (probably from a minor canting of the basically antiferromagnetic structure) is demonstrated by the size and the field dependence of the magnetization below T_N . Since the sample of **2** for magnetization measurements consists of hand-selected crystals only, the presence of ferromagnetic impurities can be (almost) excluded. The field-independence and large negative Θ of the paramagnetic susceptibility also corroborate the weak ferromagnetism of compound **2**.

Crystal Structure Determinations. $(\text{NH}_4)_{0.4}\text{Fe}^{\text{II}}_{0.55}\text{Fe}^{\text{III}}_{0.5}(\text{H}_2\text{O})_2[\text{BP}_2\text{O}_8] \cdot 0.6\text{H}_2\text{O}$ **1a**. A black crystal with a hexagonal bipyramidal shape ($0.2 \times 0.2 \times 0.2 \text{ mm}^3$) was mounted with super glue on a glass fiber. The crystal quality was first checked with precession exposures. X-ray data were collected at 293 K on a Stoe IPDS diffractometer (graphite-monochromated Ag K α radiation). Numerical absorption correction was performed on the basis of optimized shape of the crystal.¹⁸ The crystal structure was first solved in space group $P6_522$ (no. 179) by direct methods using the program SHELXS-97/2.¹⁹ Fourier calculations and subsequent full matrix least-squares refinements were carried out using SHELXL-97/2. The statistical test after Yeates²⁰ for the examination of intensity data regarding to twinning by merohedry, which is obvious for that type of space group symmetry, led to a possible pseudomerohedric twinning with a 2-fold rotation axis along [110] as the twin element and a volume fraction α -value of 0.46 (Figure 3). The test was carried out using the program TWIN 3.0.²¹ The following refinement in space group $P6_5$ (no. 170) leads to an α -value of 0.498(5) ($R1 = 0.026$; $wR2 = 0.062$ ($F_o > 4\sigma F_o$)). Due to the high correlation of parameters caused by the higher pseudosymmetry of the anionic framework, only the non-boron atoms were refined anisotropically. During the refinement, two discrete peaks inside the helical channels were observed in the difference Fourier maps and assigned to oxygen (O11) and nitrogen (N) positions. The isotropic displacement parameters for O11 and N were refined together; the sum of their occupancies was constrained to unity. Hydrogen atoms could not be located from difference Fourier maps. Further refinement details and the crystallographic data are summarized in Table 2, final atomic parameters are given in Table 3, and selected interatomic distances and angles are given in Table 5.

(18) *X-Shape 1.03: Crystal Optimization for Numerical Absorption Correction*; Stoe & Cie GmbH: Darmstadt, Germany, 1998.

(19) Sheldrick, G. M. *SHELXS-97/2: Program for the Solution of Crystal Structures and SHELXL-97/2: Program for Crystal Structure Refinement*; University of Göttingen: Germany, 1997.

(20) Yeates, T. O. *Acta Crystallogr.* **1988**, *A* **44**, 142.

(21) Kahlenberg, V.; Messner, T. *TWIN 3.0: program for testing on twinning by merohedry*; University of Bremen: Germany, 2000.

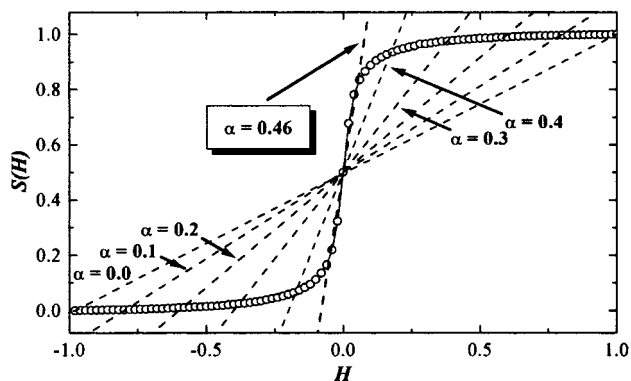


Figure 3. Yeates plot^{20,21} for **1a** (circles) compared with calculated curves for different values of the volume fraction α (dashed lines).

$\text{NH}_4\text{Fe}^{\text{III}}[\text{BP}_2\text{O}_8(\text{OH})] \cdot 2$. A pale pink rod-shaped crystal ($0.4 \times 0.1 \times 0.1 \text{ mm}^3$) was measured at 293 K using the same diffractometer. Intensity data were corrected for absorption with the same method described above. The crystal structure was solved in space group $P2_1/c$ (no. 14) using direct methods (SHELXS-97/2).¹⁹ In the refinement (SHELXL-97/2), all hydrogen atoms were located from difference Fourier maps. After non-hydrogen atoms were refined using anisotropic displacement parameters, the nitrogen-bonded hydrogen atoms were refined by applying distance and angle restraints ($R1 = 0.041$; $wR2 = 0.056$ ($F_o > 4\sigma F_o$)). Further refinement details and crystallographic data are summarized in Table 2, final atomic parameters are given in Table 4, and selected interatomic distances and angles are given in Table 6.

Results and Discussion

The crystal structure of **1a** is closely related to the family of borophosphates with the general formula $A^{\text{I}}_x\text{M}^{\text{II}}_y(\text{H}_2\text{O})_2[\text{BP}_2\text{O}_8] \cdot z\text{H}_2\text{O}$ ($A^{\text{I}} = \text{Li, Na, K, Rb, Cs}$; $\text{M}^{\text{II}} = \text{Mg, Mn, Fe, Co, Ni, Cu, Zn}$; $x = 0.35-1$, $y = 1-1.3$, $z = 0.2-1$).^{12,13} The condensation of PO_4 and BO_4 tetrahedra through common vertexes leads to ribbons $^1_{\infty}\{[\text{BP}_2\text{O}_8]^{3-}\}$, which are arranged around 6_1 or 6_5 screw axes to form chiral helices (Figure 4). The helical tetrahedral ribbons are built up from four rings of corner-sharing PO_4 and BO_4 tetrahedra. Neighboring ribbons are interconnected by $\text{M}^{\text{II}}\text{O}_4(\text{H}_2\text{O})_2$ octahedra leading to an infinite three-dimensional open-framework structure. In **1a**, the B–O distances and O–B–O angles range from 1.453 to 1.484 Å and 102.2 to 115.4°, respectively. The interatomic distances and O–P–O angles in the PO_4 tetrahedra range from 1.510 to 1.581 Å and 104.8 to 115.6°, respectively.

In comparison with the aristotype structure,¹³ the crystal structure of **1a** contains additional trigonal bipyramids $\text{Fe}^{\text{II/III}}\text{O}_2(\text{H}_2\text{O})_3$, which share common corners and edges with three $\text{Fe}^{\text{II/III}}\text{O}_4(\text{H}_2\text{O})_2$ coordination octahedra, resulting in tetrameric units (Figure 5). The Fe1–Fe2 distances range from 3.05 to 4.2 Å and the angles Fe1–Fe2–Fe1 range from 100.3 to 141.9°. A similar tetrameric building unit was also found in $(\text{NH}_4)_{0.5}\text{Co}_{1.25}(\text{H}_2\text{O})_2[\text{BP}_2\text{O}_8] \cdot 0.5\text{H}_2\text{O}$.²² Both the different iron coordination polyhedra are connected with two helical ribbons but in a different way. The Fe-centered octahedra share two corners with two PO_4 groups in each ribbon; the trigonal bipyramid shares only one

(22) Schäfer, G. Ph.D. Thesis, Darmstadt University of Technology, 2001.

Table 2. Crystallographic Data and Refinement Details for Compounds 1a and 2

compound	1a	2
space group	$P6_3$ (no. 170)	$P2_1/c$ (no. 14)
cell parameters (Å)	$a = 9.483(4)$ $c = 15.697(5)$	$a = 9.370(1)$ $b = 8.309(2)$ $c = 9.680(1)$ $\beta = 102.05(1)$
$V(\text{Å}^3)/Z$	1222.5(8)/6	737.0(2)/4
calc density ρ (g cm ⁻³)	2.514	2.628
data collection	Stoe IPDS, graphite monochromator Ag K α radiation, ϕ -scan mode	
absorption coefficient $\mu(\text{Ag K}\alpha)$ (cm ⁻¹)	12.3	13.0
ϕ -range, $\Delta\phi$, exposure time per step	0–199.8°, 0.6°, 5 min	0.0–200.0°, 1.0°, 6 min
2θ range (deg)	2.9–48.4	3.3–52.1
hkl index range	$-13 \leq h \leq 13$ $-13 \leq k \leq 13$ $-22 \leq l \leq 22$	$-14 \leq h \leq 14$ $-12 \leq k \leq 12$ $-14 \leq l \leq 14$
no. measured reflections	16 047	11 617
no. unique reflections	2589	2849
no. observed reflections $I > 2\sigma(I)$	2348	1761
$R_{\text{int}}/R_{\sigma}$	0.0335/0.0227	0.1086/0.1174
no. of refined parameters	126	138
α -value/Flack x -parameter ²⁸ (not refined) ^a	0.498(5)/–0.01(3)	
R values (reflections $F_o > 4\sigma(F_o)$)	$R1 = 0.026$ $wR2 = 0.062$	0.041 0.060
R values (all data)	$R1 = 0.032$ $wR2 = 0.064$	0.089 0.067
goodness of fit (on F^2)	1.066	0.864
residual electron density (max/min) [e Å ⁻³]	0.60/–0.37	0.76/–0.64

^a The Flack x -parameter was reset automatically after every refinement cycle. For this reason, the unrefined value was taken from the SHELXL lst file.

Table 3. Atomic Coordinates and Isotropic/Equivalent Displacement Parameters (10⁴ pm²) in the Crystal Structure of 1a

atom	x	y	z	$U_{\text{iso}}/U_{\text{eq}}$
Fe1 ^a	0.447 05(19)	0.552 21(19)	0.081 85(15)	0.011 83(8)
Fe2	0.044(2)	0.370(2)	0.2470(12)	0.042(6)
B	0.3002(3)	0.1509(13)	–0.0841(9)	0.0101(4)
P1 ^a	0.6152(3)	0.7836(3)	0.245 77(8)	0.0085(4)
P2 ^a	0.2162(3)	0.3845(3)	–0.082 42(7)	0.0103(4)
O1 ^a	0.7930(7)	0.8151(7)	0.2290(4)	0.0126(11)
O2 ^a	0.1917(7)	0.2140(7)	–0.0666(4)	0.0135(12)
O3 ^a	0.2346(8)	0.4132(8)	–0.1808(4)	0.0169(13)
O4 ^a	0.5874(7)	0.7649(7)	0.3439(3)	0.0095(10)
O5 ^a	0.4884(8)	0.6281(9)	0.2040(4)	0.0200(12)
O6 ^a	0.3769(8)	0.5130(8)	–0.0459(4)	0.0175(12)
O7 ^a	0.0679(7)	0.3859(8)	–0.0494(4)	0.0188(14)
O8 ^a	0.6813(7)	0.6165(8)	0.0452(4)	0.0187(13)
O9	0.5008(5)	0.7948(4)	0.0546(2)	0.0230(9)
O10	0.1846(4)	0.4690(5)	0.1213(2)	0.0203(7)
O11	0.1093(15)	0.1690(14)	0.2721(7)	0.077(3)
N	0.147(3)	0.262(2)	0.244(2)	0.077(3)

^a Refined with anisotropic displacement parameters.

corner with one PO₄ group in each ribbon (Figure 4). The Fe–O distances in the Fe^{II/III}O₄(H₂O)₂ coordination octahedra range from 2.016 to 2.289 Å, with the longest distances to the terminal H₂O ligands (O9 and O10). The trigonal bipyramid around Fe2 is quite deformed (2.197–2.312 Å, equatorial angles = 101.0–136.7°, axial angle = 169.8°), comparable with the trigonal bipyramidal coordinated Fe^{III} ions in [H₃N(CH₂)₂NH₃]₂Fe₄O-(PO₄)₄·H₂O²³ with Fe–O distances ranging from 1.889 to 2.387 Å.

Both water molecules (O11) and ammonium ions (N) are located inside the channels, which are formed by the helical ribbons $\frac{1}{\infty}[\text{BP}_2\text{O}_8]^{3-}$ (Figure 6 c). The statistically occupied N and O sites cannot be distin-

Table 4. Atomic Coordinates and Isotropic/Equivalent Displacement Parameters (10⁴ pm²) in the Crystal Structure of 2

atom	x	y	z	$U_{\text{iso}}/U_{\text{eq}}$
Fe ^a	0.788 16(4)	0.153 18(5)	0.570 40(5)	0.004 08(9)
B ^a	0.6667(3)	0.5627(4)	0.8096(4)	0.0065(6)
P1 ^a	0.924 51(7)	0.062 25(9)	0.295 64(8)	0.003 76(14)
P2 ^a	0.578 01(7)	0.242 72(9)	0.784 67(8)	0.004 07(14)
O1 ^a	0.9090(2)	0.1658(3)	0.4219(2)	0.0083(4)
O2 ^a	0.9229(2)	0.0059(2)	0.6917(2)	0.0081(4)
O3 ^a	0.8883(2)	0.3462(3)	0.6559(2)	0.0081(4)
O4 ^a	0.6547(2)	0.1286(2)	0.7022(2)	0.0091(4)
O5 ^a	0.5923(2)	0.4202(2)	0.7380(2)	0.0069(4)
O6 ^a	0.8145(2)	–0.0820(2)	0.2830(2)	0.0076(4)
O7 ^a	0.4104(2)	0.2107(2)	0.7447(2)	0.0082(4)
O8 ^a	0.6292(2)	0.2764(3)	0.4425(2)	0.0099(4)
O9 ^a	0.6814(2)	0.5525(3)	0.9644(2)	0.0086(4)
H1	0.610(4)	0.578(4)	0.991(4)	1.5 × $U_{\text{eq}}(\text{O9})$
N	0.8167(3)	0.5967(4)	0.438 88(4)	0.0211(7)
H2	0.827(3)	0.520(3)	0.495(3)	1.2 × $U_{\text{iso}}(\text{N})$
H3	0.875(3)	0.666(3)	0.470(3)	1.2 × $U_{\text{iso}}(\text{N})$
H4	0.734(2)	0.625(4)	0.421(3)	1.2 × $U_{\text{iso}}(\text{N})$
H5	0.840(3)	0.562(4)	0.365(3)	1.2 × $U_{\text{iso}}(\text{N})$

^a Refined with anisotropic displacement parameters.

guished directly from the X-ray data. For this reason, the distribution was obtained from the examination of interatomic distances from Fe2 to neighboring sites (Fe2–O11 = 2.312 Å and Fe2–N = 1.73 Å). The occupancies for both water molecules and ammonium ions were obtained from a constrained refinement (see the Experimental Section).

The A¹(NH₄⁺) and channel water (O11) positions are different compared with KFe(H₂O)₂[BP₂O₈]·0.5H₂O²⁴ and (NH₄)_{0.5}Co_{1.25}(H₂O)₂[BP₂O₈]·0.5H₂O²² (Figure 6). While the potassium ions are located within the free thread of the helical ribbons, the bulkier ammonium ions are located inside the channels. In 1a, the am-

(23) Huang, C.-Y.; Wang, S.-L.; Lii, K.-H. *J. Porous Mater.* **1998**, *5*, 147.

(24) Boy, I.; Schäfer, G.; Kniep, R. *Z. Kristallogr. New Cryst. Struct.* **2001**, *216*, 13.

Table 5. Crystal Structure of 1a: Selected Interatomic Distances and Angles (esd)

	distance (Å)		angle (deg)		angle (deg)		
Fe1-	O5	2.016(7)	O5-Fe1-O8	99.8(3)	O7-Fe1-O9	175.4(2)	
	O8	2.069(6)	O5-Fe1-O7	91.6(3)	O6-Fe1-O9	83.3(2)	
	O7	2.071(6)	O8-Fe1-O7	94.27(9)	O5-Fe1-O10	81.3(2)	
	O6	2.087(6)	O5-Fe1-O6	164.83(11)	O8-Fe1-O10	177.4(2)	
	O9	2.136(4)	O8-Fe1-O6	89.1(3)	O7-Fe1-O10	83.4(2)	
	O10	2.289(4)	O7-Fe1-O6	100.0(3)	O6-Fe1-O10	90.2(2)	
			O5-Fe1-O9	84.7(2)	O9-Fe1-O10	93.34(13)	
			O8-Fe1-O9	89.1(2)			
	Fe2-	O9	2.139(17)	O9-Fe2-O6	101.0(7)	O8-Fe2-O10	169.8(8)
		O6	2.197(17)	O9-Fe2-O8	77.8(6)	O9-Fe2-O11	117.4(8)
O8		2.251(19)	O6-Fe2-O8	81.9(6)	O6-Fe2-O11	136.7(8)	
O10		2.300(18)	O9-Fe2-O10	107.0(8)	O8-Fe2-O11	87.0(7)	
O11		2.312(19)	O6-Fe2-O10	88.3(6)	O10-Fe2-O11	98.3(7)	
B-	O2	1.453(10)	O2-B-O3	112.9(9)	O3-B-O4	102.15(18)	
	O3	1.464(12)	O2-B-O1	102.37(19)	O1-B-O4	111.6(9)	
	O1	1.480(10)	O3-B-O1	115.4(9)			
	O4	1.483(12)	O2-B-O4	112.9(9)			
P1-	O5	1.510(7)	O5-P1-O8	113.3(4)	O8-P1-O1	105.0(3)	
	O8	1.528(6)	O5-P1-O4	108.2(4)	O4-P1-O1	106.9(3)	
	O4	1.557(6)	O8-P1-O4	111.9(3)			
	O1	1.581(6)	O5-P1-O1	111.5(4)			
P2-	O7	1.505(6)	O7-P2-O6	115.6(4)	O6-P2-O3	104.8(4)	
	O6	1.510(7)	O7-P2-O2	107.7(3)	O2-P2-O3	106.8(4)	
	O2	1.534(6)	O6-P2-O2	110.4(4)			
	O3	1.563(7)	O7-P2-O3	111.2(4)			

Table 6. Crystal Structure of 2: Selected Interatomic Distances and Angles (esd)

	distance (Å)		angle (deg)		angle (deg)	
Fe-	O3	1.953(2)	O3-Fe-O2	93.81(9)	O4-Fe-O1	174.17(9)
	O2	1.962(2)	O3-Fe-O4	97.13(9)	O8-Fe-O1	89.33(9)
	O4	1.975(2)	O2-Fe-O4	87.95(9)	O3-Fe-O9	176.34(9)
	O8	2.007(2)	O3-Fe-O8	94.09(9)	O2-Fe-O9	88.08(9)
	O1	2.010(2)	O2-Fe-O8	171.46(9)	O4-Fe-O9	86.06(9)
	O9	2.132(2)	O4-Fe-O8	87.87(9)	O8-Fe-O9	84.20(9)
			O3-Fe-O1	88.16(9)	O1-Fe-O9	88.58(9)
			O2-Fe-O1	94.15(9)		
			O7-B-O6	104.9(2)	O6-B-O9	107.0(2)
B-	O6	1.469(4)	O7-B-O5	110.9(2)	O5-B-O9	111.4(2)
	O5	1.472(4)	O6-B-O5	112.1(2)		
	O9	1.478(4)	O7-B-O9	110.3(2)		
			O2-P1-O1	113.01(12)	O1-P1-O6	108.80(12)
P1-	O1	1.526(2)	O2-P1-O3	106.79(11)	O3-P1-O6	106.88(12)
	O3	1.527(2)	O1-P1-O3	112.83(12)		
	O6	1.569(2)	O2-P1-O6	108.27(11)		
P2-	O8	1.511(2)	O8-P2-O4	112.45(12)	O4-P2-O7	109.05(12)
	O4	1.514(2)	O8-P2-O5	111.38(12)	O5-P2-O7	103.45(11)
	O5	1.556(2)	O4-P2-O5	111.19(12)		
	O7	1.560(2)	O8-P2-O7	108.89(12)		

Hydrogen bonds

N...O3	2.934	N-H2...O3	170
N...O1	3.298	N-H3...O1	169
N...O7	2.943	N-H4...O7	137
N...O4	3.099	N-H5...O4	117
N...O2	2.904	N-H5...O2	172

monium ions are shifted closer to the inner wall of the helical channels, compared with $(\text{NH}_4)_{0.5}\text{Co}_{1.25}(\text{H}_2\text{O})_2\text{[BP}_2\text{O}_8]\cdot 0.5\text{H}_2\text{O}$,²² because of the lower occupancy of the five-coordinated metal site ($\text{Fe}^{\text{II}}/\text{Fe}^{\text{III}}$ vs Co^{II} for charge compensation). The positions of water molecules inside the helical channels in **1a** and the ammonium-cobalt borophosphate are similar. In the case of $\text{KFe}(\text{H}_2\text{O})_2\text{[BP}_2\text{O}_8]\cdot 0.5\text{H}_2\text{O}$,²⁴ the water molecules inside the helical channels are closer to the central screw axes because of the longer bond distance of $\text{K}-\text{O}_{\text{H}_2\text{O}}$ (2.624(3) Å) compared with the bond distances of $\text{Fe}2-\text{O}11$ (2.312(19) Å) in **1a** and $\text{Co}-\text{O}_{\text{H}_2\text{O}}$ (2.176(24) Å) in $(\text{NH}_4)_{0.5}\text{Co}_{1.25}(\text{H}_2\text{O})_2\text{[BP}_2\text{O}_8]\cdot 0.5\text{H}_2\text{O}$.²² Furthermore, the positions of A^{I} ions in $\text{A}^{\text{I}}\text{M}^{\text{II}}(\text{H}_2\text{O})_2\text{[BP}_2\text{O}_8]\cdot z\text{H}_2\text{O}$ ($\text{A}^{\text{I}} = \text{Li, Na, K; M}^{\text{II}} = \text{Mg, Mn, Fe, Co, Ni, Cu, Zn; } z = 0.5-1$)^{12,13,24} and the partially occupied Fe and Co

sites in **1a** and $(\text{NH}_4)_{0.5}\text{Co}_{1.25}(\text{H}_2\text{O})_2\text{[BP}_2\text{O}_8]\cdot 0.5\text{H}_2\text{O}$ ²² are within the free thread of the helical ribbons ${}_{\infty}^1\{\text{[BP}_2\text{O}_8]^{3-}\}$ (Figure 6) and, therefore, stabilize the borophosphate ribbon and vice versa.

Recently, Yilmaz et al. reported a "black" isotopic compound with the formula $\text{Fe}(\text{H}_2\text{O})_2\text{[BP}_2\text{O}_8]\cdot \text{H}_2\text{O}$ as a pure Fe^{III} borophosphate.¹⁵ The compound was prepared under the same reaction conditions as reported here, using $(\text{NH}_4)_2\text{HPO}_4$ as one of the starting materials. The crystal structure was refined in the space group $P6_322$ (no. 179), resulting in an uncommonly large displacement parameter for site $\text{O}6_{\text{H}_2\text{O}}$ ($U_{\text{eq}} = 0.276(9) \text{ \AA}^2$), assigned to a fully occupied site in the helical channels.

The large U_{eq} for $\text{O}6$ may indicate vacancies or positional disorder. In our structure refinement, this

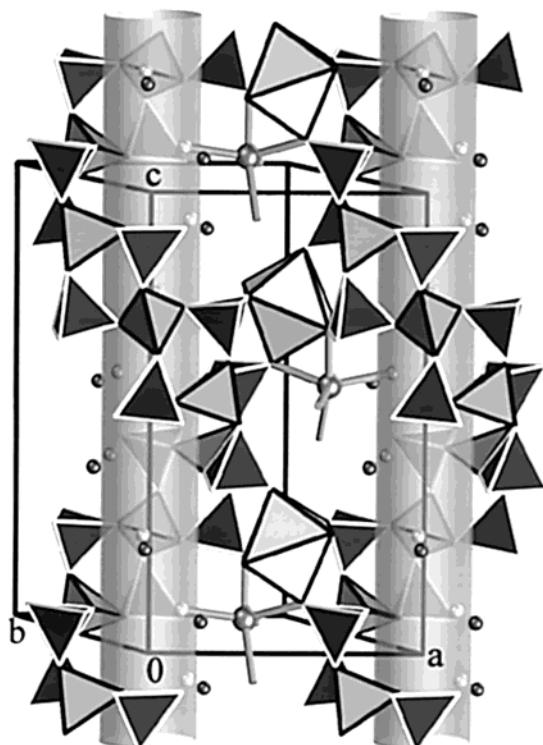


Figure 4. Crystal structure of **1a**: linkage of the borophosphate helices (BO₄ tetrahedra, gray; PO₄ tetrahedra, dark gray; Fe^{II}/Fe^{III}O₆(H₂O)₂ octahedra, gray; Fe2 site, large gray spheres; O11H₂O, gray spheres; N_{NH₄⁺, black spheres).}

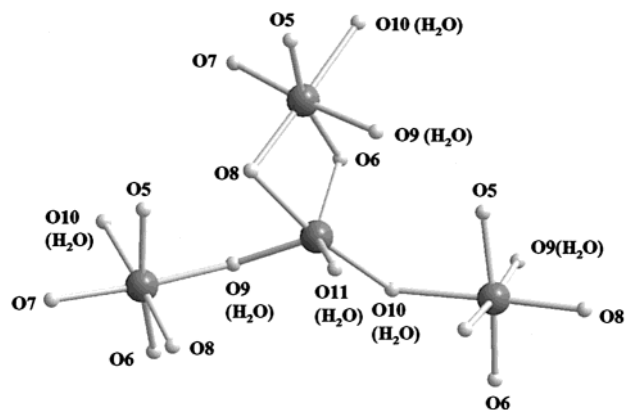


Figure 5. Tetrameric unit of iron coordination polyhedra in the crystal structure of **1a**.

“O6 site” was described as two adjacent positions, partially occupied by N(NH₄⁺) and O11(H₂O), and being refined with more acceptable U_{eq} .

In our compounds **1a** and **1b**, the presence of ammonium ions (confirmed by IR spectroscopy, chemical analysis, and thermal analysis) is needed because iron is present in both valence states Fe^{II} and Fe^{III}. The mixed-valence state of iron is also reflected in the black color of the crystals of **1a** and pale gray color of **1b** and their magnetic moments.

The IR spectrum of Fe^{III}(H₂O)₂[BP₂O₈]·H₂O was also measured by Yilmaz,²⁵ but it was presented without interpretation at all. In fact, the IR spectrum shows a line at 1420 cm⁻¹, typical for a ν_4 (N–H) deformation vibration, which demonstrates the presence of NH₄⁺ in

Fe^{III}(H₂O)₂[BP₂O₈]·H₂O. A three-step mass loss in the TG curve with the third mass loss step in the temperature range between 500 and 600 °C was also given in the respective thesis²⁵ (a two-step mass loss in the temperature range of 100–500 °C was given in the paper¹⁵). No results of chemical analyses are given, either in the paper or in the thesis, to prove the absence of nitrogen. Furthermore, an inconsistency concerning the magnetic susceptibility data in the paper¹⁵ should be pointed out; the Weiss constant Θ should be about –4 K instead of –25 K, according to the plot for the temperature dependence of $1/\chi$ (Figure 4 and the linear equation given in the same plot in ref 15). According to our results, the so-called Fe^{III} compound, “Fe(H₂O)₂·[BP₂O₈]·H₂O”,¹⁵ is not a pure Fe^{III} compound; its black color already reveals the mixed valence state of iron (Fe^{II}/Fe^{III}).^{17,23,26} But the main question that arises is about the completely empty position within the free thread of the helical borophosphate ribbons in Fe(H₂O)₂·[BP₂O₈]·H₂O.¹⁵ According to our results, this position should be filled, at least partially, by positively charged ions to stabilize the helical borophosphate ribbon. We did not observe Fe(H₂O)₂[BP₂O₈]·H₂O¹⁵ in any of our reactions; instead, we obtained the pale pink colored NH₄Fe^{III}[BP₂O₈(OH)] **2**.

The compound **2** was observed first as a byproduct during the synthesis of the above compound **1a/1b**. It is an isotype of the borophosphates M^IM^{III}[BP₂O₈(OH)] (M^I = Rb, Cs; M^{III} = V, Fe).¹⁶ The anionic partial structure contains an open-branched vierer-single chain $\infty\{[BP_2O_8(OH)]^{4-}\}$ (Figure 7), which is formed by alternating corner-sharing BO₃OH and PO₄ tetrahedra with a further dangling PO₄ tetrahedra bonded to the BO₃OH group. Boron is in a nearly regular tetrahedral coordination with B–O distances ranging between 1.467 and 1.478 Å and angles ranging from 104.9 to 112.1°. For P1, the P–O distances range from 1.519 to 1.569 Å and the O–P–O angles range from 106.8 to 113.0°. For P2, the P–O distances range from 1.511 to 1.560 Å and the O–P–O angles range from 103.5 to 112.5°. The Fe–O distances range from 1.953 to 2.132 Å. Two $\infty\{[BP_2O_8(OH)]^{4-}\}$ chains are connected by FeO₅(OH) octahedra, leading to a one-dimensional channel system (Figure 8, channel size derived from crystallographic O···O distances $\approx 4.70 \times 4.76$ Å²). The channels are occupied by ammonium ions connected by hydrogen bonds with the anionic $\infty\{[Fe[BP_2O_8(OH)]^{-}]\}$ framework (N···O distances between 2.904 and 3.298 Å and N–H···O angles ranging from 117.3 to 172.5°).

Conclusions

The title compounds **1a**, **1b**, and **2** have been synthesized by mild hydrothermal methods. The Yeates test²⁰ showed that the crystals of **1a** exhibit twinning by merohedry. The oxidation states of iron in these compounds **1a** and **1b** have a remarkable flexibility, depending on the preparation conditions, as confirmed by product color (ranging from black to pale gray) and measurement of magnetic susceptibilities. This indicates, together with small variations in the chemical composition (Table 1), the presence of a homogeneity

(25) Yilmaz, A. Ph.D. Thesis, Middle East Technical University, Ankara, 2000.

(26) Moore, P. B. *Am. Mineral.* **1979**, *55*, 135.

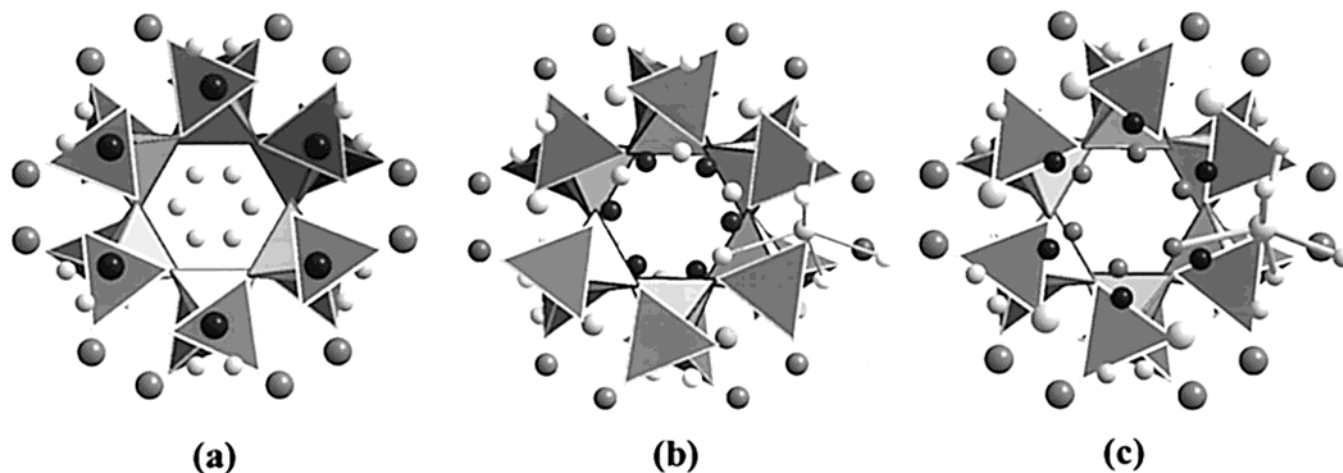


Figure 6. Helical arrangements in the crystal structures of $\text{KFe}(\text{H}_2\text{O})_2[\text{BP}_2\text{O}_8] \cdot 0.5\text{H}_2\text{O}$ (a),²⁴ $(\text{NH}_4)_{0.5}\text{Co}_{1.25}(\text{H}_2\text{O})_2[\text{BP}_2\text{O}_8] \cdot 0.5\text{H}_2\text{O}$ (b),²² and $(\text{NH}_4)_{0.4}\text{Fe}^{\text{II}}_{0.55}\text{Fe}^{\text{III}}_{0.5}(\text{H}_2\text{O})_2[\text{BP}_2\text{O}_8] \cdot 0.6\text{H}_2\text{O}$ (**1a**) (c); view along [001]. (BO_4 tetrahedra, gray; PO_4 tetrahedra, dark gray; A^{I} and NH_4^+ ions, black spheres; octahedral coordinated M^{II} ions, dark gray spheres; five-coordinated M^{II} ions, gray spheres; water molecules, small gray spheres).



Figure 7. Open-branched vierer-single chain $\frac{1}{4}[\text{BP}_2\text{O}_8(\text{OH})]^{4-}$ in the crystal structure of **2** (BO_4 tetrahedra, gray; PO_4 tetrahedra, dark gray; H, small pale gray spheres).

range. The ratio of the charge balancing cations NH_4^+ and $\text{Fe}^{\text{II}}/\text{Fe}^{\text{III}}$, together with the content of water inside the helical channels, shows some flexibility. One reason for the homogeneity range should be the ratio of $\text{Fe}^{\text{II}}/\text{Fe}^{\text{III}}$. The family of borophosphates with the general composition $\text{A}^{\text{I}}_x\text{M}^{\text{II}}_y(\text{H}_2\text{O})_z[\text{BP}_2\text{O}_8] \cdot z\text{H}_2\text{O}$ ($\text{A}^{\text{I}} = \text{Li}, \text{Na}, \text{K}, \text{Rb}, \text{Cs}$; $\text{M}^{\text{II}} = \text{Mg}, \text{Mn}, \text{Fe}, \text{Co}, \text{Ni}, \text{Cu}, \text{Zn}$; $x = 0.35-1$, $y = 1-1.3$, $z = 0.2-1$)^{12,13} is known now for not only its flexibility in accommodating various A^{I} and M^{II} species and the position of A^{I} sites as a function of its size but also the substitution of the M^{II} site by $\text{Fe}^{\text{II}}/\text{Fe}^{\text{III}}$ correlated with the lower occupancy of the A^{I} site, as demonstrated. A second mixed valent iron compound with $\text{A}^{\text{I}} = \text{Rb}$ ($\text{Rb}_x\text{Fe}^{\text{II}}_x\text{Fe}^{\text{III}}_{1-x}(\text{H}_2\text{O})_2[\text{BP}_2\text{O}_8] \cdot z\text{H}_2\text{O}$) was described recently.²⁷ A complete substitution of Fe^{II} by Fe^{III} , as described in ref 15, was not observed in our experiments. A complete substitution of Fe^{II} by Fe^{III} leads to holes within the helical borophosphate ribbons and, thus, to a destabilization of the whole crystal structure. Instead, we observed another pure Fe^{III} compound with the formula $\text{NH}_4\text{Fe}^{\text{III}}[\text{BP}_2\text{O}_8(\text{OH})]$ **2**.

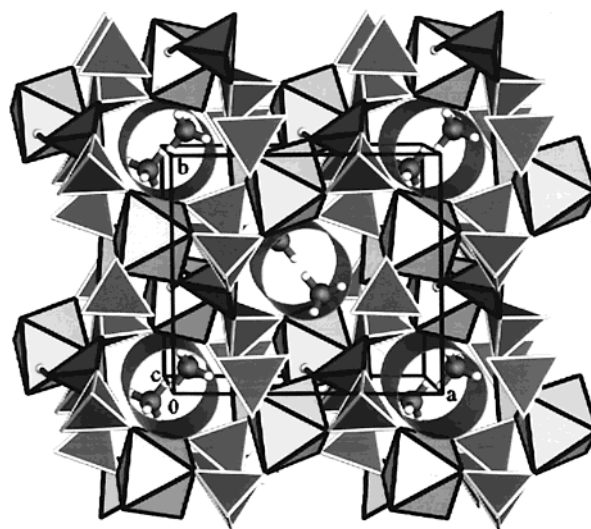


Figure 8. Crystal structure of $\text{NH}_4\text{Fe}^{\text{III}}[\text{BP}_2\text{O}_8(\text{OH})]$ (**2**). The one-dimensional channel system, running along [100], is emphasized by the tubes (BO_4 tetrahedra, gray; PO_4 tetrahedra, dark gray; $\text{Fe}^{\text{III}}\text{O}_4(\text{H}_2\text{O})_2$ octahedra, gray; N, dark gray spheres; H, small pale gray spheres).

Acknowledgment. This work was supported by the Pinguin-Stiftung (Düsseldorf) and the Fonds der Chemischen Industrie. Y.-X. Huang gratefully acknowledges the Max Planck Society for a fellowship. We thank Mrs. B. Beyer for chemical analyses, Mrs. S. Müller for thermal analyses, and Dr. Yu. Grin (MPI-CPfS) and Dr. H. D. Flack (University of Geneva) for fruitful discussions.

Supporting Information Available: CIF files for compounds **1a** and **2**. This material is available free of charge via the Internet at <http://pubs.acs.org>.

(27) Engelhardt, H. Ph.D. Thesis, Darmstadt University of Technology, 2000.

(28) Flack, H. D. *Acta Crystallogr.* **1983**, *A* **39**, 876.